Estuarine, Coastal and Shelf Science 280 (2023) 108182

Contents lists available at ScienceDirect

Estuarine, Coastal and Shelf Science

journal homepage: www.elsevier.com/locate/ecss

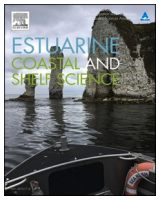

Temporal variability of phytoplankton biomass and net community production in a macrotidal temperate estuary

Africa P. Gomez-Castillo *, Anouska Panton, Duncan A. Purdie

School of Ocean and Earth Science, University of Southampton, National Oceanography Centre, European Way, Southampton, SO14 3ZH, UK

ARTICLE INFO

Keywords:
Estuarine ecosystems
High-frequency data
Dissolved oxygen
Net community production
Phytoplankton blooms

ABSTRACT

Coastal zones play a significant role in Earth's biogeochemical processes. Within these regions, estuaries are particularly important due to their complex ecological interactions and spatial and temporal variability. The aim of this study was to apply a year long high-frequency (15 min) environmental data time series to identify both the timing and factors influencing phytoplankton blooms in the Southampton Water estuary. Dissolved oxygen measurements from an *in situ* deployed optode were applied to the open diel oxygen method to estimate daily integrated rates of gross primary production (GPP), ecosystem respiration (ER) and net community production (NCP). Additional water quality data including temperature, salinity, chlorophyll concentration and turbidity allowed the relationship between physical and biological processes occurring over different time scales to be investigated. The occurrence of major phytoplankton blooms during the spring-summer period were associated with critical values of estuarine water temperature and mean water column irradiance. In addition, neap tides were found to promote the initiation of phytoplankton blooms in late spring and summer months. Annual daily average NCP for the estuarine ecosystem presented an estimated net heterotrophic state (-0.8 mmol O_2 m^{-2} d^{-1}), although seasonal productivity events shifted this state for several days and sometimes weeks to net autotrophic conditions. The results of this study have demonstrated how high frequency *in situ* dissolved oxygen measurements from an optode can make a valuable contribution to understanding the key factors influencing bloom events in a temperate macrotidal estuary. This approach if applied more widely to other coastal sites could therefore contribute to consolidating global annual primary production budgets for coastal regions.

1. Introduction

Coastal zones represent around 7% of the total ocean surface area (Kanuri et al., 2017), however, they are responsible for 14–33% of total oceanic production (Garcia-Corral et al., 2021). Within these regions, estuaries play a major role in hydrographic and biogeochemical processes of marine ecosystems (Mahoney and Bishop, 2017; Ruiz-Ruiz et al., 2017) due to the mixing of riverine freshwater with seawater carried in by the tides (Srichandan et al., 2015).

Given that phytoplankton communities form the base of most marine ecosystems (Leterme et al., 2014), the phytoplankton biomass distribution in an estuary can indicate the dynamics of the seasonal and annual variability of the system properties such as water quality and the aquatic trophic state (Cloern and Jassby, 2010; Haskell et al., 2019).

Several techniques are used to determine aquatic rates of net primary production, the most common being measurements of radioactive carbon 14 isotope ($^{14}CO_2$) incorporation by a natural community of microplankton incubated in bottles (Oczkowski et al., 2016). Alternatively, changes in dissolved oxygen (DO) can be measured in small volume glass bottle incubations in the dark and light to define rates of planktonic respiration and net production (Langdon and Garcia-Martin, 2021). The problems inherent in these short term, small volume incubation techniques however are exacerbated in the highly dynamic heterogeneous coastal zone, where the seasonal oxygen change shows marked variability (Queste et al., 2016). Interaction between physical and biological processes within estuaries tends to vary over diurnal, semi-diurnal and sometimes episodic timescales, making acquiring frequent data critical to accurately assess ecosystem health for these periods (Bianchi, 2012; Nidzieko et al., 2014).

An alternative, more integrative, method to estimate primary production relies on the calculation of the *in situ* oxygen mass-balance from continuous measurements of DO, the open diel oxygen water method, first proposed by Odum (1956) and later modified to apply it to estuarine systems (Caffrey, 2003, 2004; Emerson et al., 2008). This method

* Corresponding author.
E-mail address: A.P.Gomez-Castillo@soton.ac.uk (A.P. Gomez-Castillo).

https://doi.org/10.1016/j.ecss.2022.108182
Received 19 August 2022; Received in revised form 29 November 2022; Accepted 5 December 2022
Available online 9 December 2022

quantifies the *in situ* diel oscillations in DO concentration to estimate daily integrated gross primary production (GPP), ecosystem respiration (ER) and net community production (NCP), also known as net ecosystem metabolism (Demars et al., 2015).

NCP is a community-level process that integrates all processes affecting the balance between GPP and ER (Duarte & Regaudie-De-Gioux, 2009; Garcia-Corral et al., 2021). If the NCP estimation is positive, the ecosystem is considered net autotrophic and exports or stores the excess organic carbon and is a potential sink for atmospheric CO_2. Conversely, a net heterotrophic ecosystem is characterised by a negative NCP that requires stored or imported organic matter to maintain its metabolic state and acts as a net CO_2 source (Feng et al., 2012; Nidzieko et al., 2014).

The aim of this study was to estimate daily and seasonal changes in estuarine primary production and identify the environmental factors influencing its variability by using continuous high-frequency environmental data in the macrotidal Southampton Water estuary, over a period of one year. To our knowledge, this is the first study to apply high-resolution oxygen diel data to calculate productivity rates and relate them to phytoplankton blooms in a UK estuarine system. While our study is regional, the heterogeneity of coastal zones is of global concern and results from this study will allow a better understanding of local and regional primary production dynamics as well as provide a baseline to assess future anthropogenic impacts and climate change alterations to the aquatic trophic state of the Southampton Water estuary.

2. Materials and methods

2.1. Study sites

The Southampton Water estuary is part of the Solent estuarine system, considered the largest on the south coast of the UK (Fig. 1). It is an approximately linear body of water about 2 km wide and 10 km long with a central channel continuously dredged to a minimum depth of 12.2 m below the local Chart Datum. Three main rivers discharge into Southampton water: the River Test and Itchen towards the head of the estuary and the river Hamble, nearer to the mouth on the eastern side (Iriarte and Purdie, 2004).

The estuary is characterised by a semi-diurnal tidal regime where each tide consists of a double high water, ~2 h apart, followed by a short ebb-tide. The tidal range varies between 1.5 m on neaps and 5.0 m on springs (Crawford et al., 1997). It is considered a partially mixed system, with minimal stratification occurring throughout the semi-diurnal tidal cycle with the highest vertical density gradient occurring at low water and well-mixed conditions at high water (Levasseur et al., 2007).

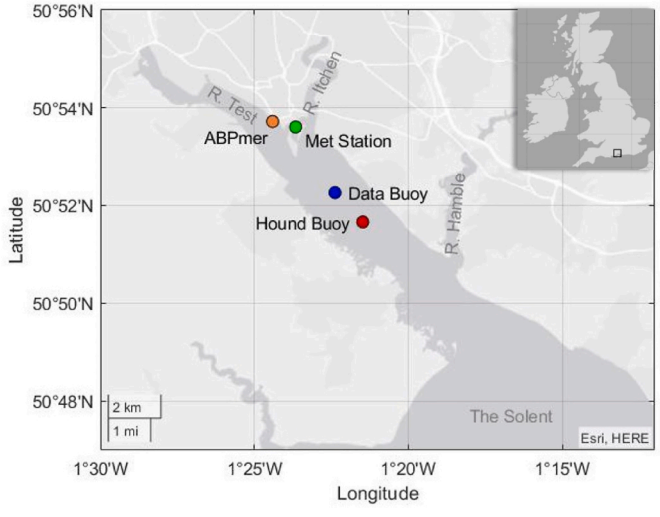

Fig. 1. Map of the Southampton Water estuary located on the south coast of The UK (inset). Data sets were collected from the Meteorological station at the National Oceanography Centre (green circle ●), tide gauge data from ABP Marine Environmental Research (orange circle ●), Xylem Analytics Data Buoy system (blue circle ●) and Environment Agency samples from Hound navigation buoy (red circle ●). (For interpretation of the references to colour in this figure legend, the reader is referred to the Web version of this article.)

2.2. Data sources

Water quality data were collected using a YSI EXO2 sonde deployed since 2018 on a solar-powered Xylem Analytics UK EMM700 Data Buoy located at 50.871° N, −1.373° W, in the Southampton Water estuary (Fig. 1). The sonde was placed into an open flow PVC tube fixed to the Data Buoy at a depth of 1.6 m below the sea surface; the average water depth at the site was 10 m. Parameters recorded by the sonde included dissolved oxygen (DO) concentration (mg L^{-1}) and oxygen saturation (%), temperature (°C), salinity, chlorophyll '*a*' (μg L^{-1}) and turbidity (FNU). The sonde is connected to a Storm data logger situated within the Data Buoy system that regularly uploads data, via a mobile phone connection, to a dedicated webpage within the Storm Central cloud data collection service (https://stormcentral.waterlog.com/). Data was recorded at high-frequency (every 15 min) from January 2019 to December 2019, but with hourly averages calculated for the purpose of this study. Two gaps in data collection occurred: the first between 13/02/2019 and 19/03/2019, caused by the sonde being recovered while the Data Buoy mooring chain was replaced and the sonde and PVC tube cleaned of biofouling and the second gap from 23/11/2019 to 04/12/2019 due to some problems backfilling data when the Storm Central server migrated from one IP address to another. All data was carefully inspected for unreliable values, and outliers plus negative or occasional inconsistent high magnitude values (typically caused by biofouling) were discarded manually.

The Data Buoy system was originally fitted with a multi-parameter weather station, but this stopped recording on 12/09/18 due to damage from a boat collision. Hourly barometric pressure measurements during 2019 were taken from a Met Office meteorological station mounted on the roof of the National Oceanography Centre (archived in the Met Office's MIDAS database). Additionally, the National Oceanography Centre meteorological database was used to obtained hourly wind speed and solar radiation values, measured at the same site (50.892° N, −1.394° W).

A set of water quality measurements from the Southampton Water estuary was acquired from the Environment Agency Water Quality Archive (https://environment.data.gov.uk/water-quality/view/download/new). Data from the Hound navigation Buoy sampling site (50.861° N, −1.358° W) was selected to compare with the Xylem Analytics Data Buoy measurements due to its close proximity. Environment Agency data included monthly surface records of DO (mg L^{-1} and % sat.), temperature (°C), salinity (psu), chlorophyll '*a*' (μg L^{-1}), and turbidity (FNU).

The Associated British Ports (ABP) Marine Environmental Research provided minute-interval sea surface elevation data measured with a Tidalite tide gauge located at Dock Head, Eastern Docks Southampton (Fig. 1). Daily minimum and maximum values were extracted from the raw time series, and the difference plotted to indicate changes in the daily tidal range.

2.3. Field sampling

Discrete water samples were periodically collected using a Niskin bottle deployed at 2 m below the sea surface close to the Data Buoy from the RV *Callista*. Sets of three replicate glass bottles (~60 ml) were filled from the Niskin to measure DO concentration on several dates during winter and spring 2019. The chemical determination of oxygen concentration was based on the method first proposed by Winkler (1888) and modified by Parsons et al. (1984). Winkler titrations were

performed using a photometric end-point detector (Carrit and Carpenter, 1966).

Surface water samples for phytoplankton analysis were collected biweekly from the data buoy and 100 ml added to a darkened glass bottle and preserved in acidic Lugol's iodine to a final concentration of 1%. For analysis, 10 ml of preserved sample was settled in a glass sedimentation chamber for 24 h and cells then identified and counted using a Leica inverted light microscope (Utermöhl, 1958). Samples for later nutrient analysis were filtered through a 25 mm diameter GF/F filter using an inline syringe unit and then frozen in 50 ml plastic bottles prior to analysis. Concentrations of nitrate plus nitrite, phosphate and silicate were determined on a QuAAtro segmented flow nutrient analyser (SEAL Analytical, UK) as described by Panton et al. (2020).

2.4. Mean water column irradiance

Photosynthetic Active Radiation (PAR) within the water column varies according to changes in surface incident solar irradiance, turbidity, and depth (Cloern et al., 2014). Therefore, the mean water column irradiance (I_m) was calculated following Riley (1967) as:

$$I_m = I_0 \frac{(1 - e^{-k_{PAR}h})}{k_{PAR}h} \quad (1)$$

where I_0 is the daily surface irradiance (W h m^{-2} d^{-1}), k_{PAR} is the diffuse attenuation coefficient (m^{-1}), and h is the mixed layer depth (10 m). The diffuse attenuation coefficient was estimated from the slope of a linear regression of turbidity against k_{PAR} data previously generated for the estuary by Iriarte and Purdie (2004), with k_{PAR} ranging between 0.2 and 2.0 m^{-1}.

2.5. Optode-based oxygen sensor validation

Semi-continuous oxygen measurements were determined from the EXO2 sonde deployed optode. While optodes have proven useful in describing biogeochemical processes (Bittig and Körtzinger, 2015), to ensure high quality dissolved oxygen data were being recorded, we compared the optode data to measurements made on discrete water samples (Haskell et al., 2019; Uchida et al., 2008). The following correction steps were therefore made prior to using the oxygen time-series data to calculate NCP rates: (i) Some missing salinity measurements from the time series were estimated since the optode DO sensor installed on the EXO2 sonde measures oxygen saturation and then salinity and temperature data are used to calculate DO concentration. During 2019, the salinity sensor on the sonde showed some periods of drifting, and a more reliable sensor was not replaced until November. Thus, Environment Agency measured salinity data was compared against existing and reliable salinity data from the EXO2 sonde, and an equation from that correlation was used to substitute missing salinity data. (ii) Recalculating DO concentration values from polynomial temperature and salinity dependant equations (Feistel, 2008). (iii) Lastly, discrete oxygen measurements from Winkler titrations and Environment Agency collected measurements were used to formulate a standard linear regression (see supplementary material Fig. A1) model to correct optode derived DO concentration values.

2.6. Open diel oxygen method

The open diel method (Needoba et al., 2012) was applied to calculate daily NCP by calculating oxygen mass-balance in the surface mixed layer (see supplementary material). An essential assumption of this model is that all measurements come from a well-mixed water column; therefore, the water mass recorded presents the same metabolic history (Caffrey et al., 2014).

The hourly biological oxygen production (BOP) calculation incorporated equations used by Hull et al. (2016) and Murrell et al. (2018). In Eq. (2) C_0 is the oxygen concentration at $t = 0$ and C_1 oxygen concentration at the time step (for the present study, 1 h), and it is analytically solved by using the air-sea diffusion flux calculation F and a transfer velocity correction t, caused by wind-induced turbulence in the mixed water column (h).

$$BOP = th\left(\frac{C_1 - C_0}{1 - e^{-rt}} + C_0\right) - Fh \quad (2)$$

The diffusive exchange of gases across the air– sea interface F (Eq. (3)) was calculated as a function of gas transfer velocity k_w (Eq. (4)) and diffusion through bubbles B. P_{atm} corresponds to an atmospheric pressure standard value of 101,325 Pa, P_{slp} is the atmospheric air pressure at sea level, C^* is the calculated oxygen concentration in equilibrium with the atmosphere as a function of temperature and salinity (Feistel, 2008) and C is the oxygen concentration in the surface mixed layer.

$$F = \frac{k_w}{h} C^* (1 + B) \frac{P_{slp}}{P_{atm}} + \frac{1}{h} \frac{\partial h}{\partial t} C \quad (3)$$

k_w (Eq. (4)) is the parameterisation proposed by Wanninkhof (2014), as function of salinity and temperature through the relation between the Schmidt number Sch_{O_2} for oxygen and the normalised Schmidt number for CO_2 at 20 °C and salinity of 35 (constant value of 660 in Eq. (4)). U corresponds to wind speed measured at 10 m above sea level but as stated above can be considered the same as at sea level at the position of the Data Buoy.

$$k_w = 0.251 U^2 \left(\frac{Sch_{O_2}}{660}\right)^{-0.5} \quad (4)$$

BOP data were averaged separately into "day" and "night" periods using light data from the MIDAS Met station. Respiration rates were assumed to be constant during a diel cycle; thus, respiration was extrapolated to 24 h to obtain daily ecosystem respiration (*ER*). Finally, daily *NCP* (Eq. (5)) was calculated as a function of the difference between daily gross primary production (*GPP*) and ER.

$$NCP = GPP - ER \quad (5)$$

When calculations produce anomalous results (either negative GPP or positive ER), those values are discarded (Caffrey, 2003; Caffrey et al., 2014).

2.7. Statistical analysis

None of the environmental data nor productivity rates were normally distributed, despite different transforms being applied. Consequently, the non-parametric Spearman's Rank-Order Correlation Coefficient ($p < 0.05$) was used to evaluate the strength of associations among calculated productivity rates and measured environmental variables throughout the study period (Table 1). Data were divided into separate groups (Table 2), and the Kruskal-Wallis One Way Analysis of Variance on Ranks ($p < 0.05$) and the all pairwise Dunn's test ($p < 0.05$) were used to evaluate whether environmental conditions and productivity rates changed between major bloom event periods and the remaining days over the 12-month period. In order to explain the sources of variability in bloom events, Principal Component Analysis was applied. This method allows reducing the dimensionality of large datasets without losing its variability by transforming original variables into a new and smaller set of uncorrelated variables (Jollife and Cadima, 2016). Statistical analysis was performed using the statistical package in SigmaPlot version 13.0.

3. Results

3.1. Variation of environmental conditions

The estuarine water temperature reflected a seasonal warming, with

Table 1
Spearman's correlation coefficients relating environmental conditions and productivity rates. Including mean water column irradiance I_m (W h m^{-2} d^{-1}), tidal range (Tidal), wind speed (Wind), temperature (Temp.), salinity (Sal.), dissolved oxygen saturation (O_2%) and concentration ([O_2]), chlorophyll '*a*' (Chl '*a*'), turbidity (Turb.), net community production (NCP), gross primary production (GPP) and ecosystem respiration (ER).

	I_m	Tidal	Wind	Temp.	Sal.	O_2%	[O_2]	Chl '*a*'	Turb.
NCP	**0.61**	−0.10	**−0.15**	**0.24**	**−0.19**	**0.60**	**0.37**	**0.61**	**−0.43**
GPP	**0.40**	−0.10	**0.47**	**0.41**	0.10	**0.28**	**0.12**	**0.57**	**−0.15**
ER	**0.21**	−0.00	**−0.66**	**−0.12**	**−0.22**	**0.27**	**0.15**	0.04	**−0.24**

Values in bold $p < 0.05$. Values underlined represent absolute coefficient with strong correlation, $\rho > 0.55$.

Table 2
Average and range of daily measured environmental conditions and calculated productivity rates for different major bloom events (continuous chlorophyll '*a*' concentration values higher than 10 μg L^{-1}) and low productivity period LPP (studied days without blooms).

	I_m	Tidal range	Wind speed	Temp.	Sal.	O_2%	[O_2]	Chl '*a*'	Turb.	NCP	GPP	ER
LPP	221.7[a]	3.3[a]	4.3	12.7[a]	31.7[a]	95.9[a]	274.8[a]	0.9[a]	5.4[a]	−21.2[a]	18.0[a]	−39.3[a]
	(26.9 : 2001.9)	(1.6 : 4.8)	(1.1 : 13.1)	(5.7 : 22.0)	(28.8 : 33.6)	(81.5 : 116.9)	(205.8 : 361.4)	(0.1 : 3.3)	(1.8 : 10.9)	(-366.8 : 91.9)	(0.2 : 117.9)	(-437.5: -0.2)
Bloom 1	625.1[b]	3.0[ab]	4.2	12.9[a]	31.3[a]	120.6[b]	330.7[b]	4.2[b]	3.8[a]	59.9[b]	110.2[b]	−50.3[a]
(111–124)	(188.3 : 1337.6)	(1.7 : 4.4)	(2.0 : 8.9)	(12.3 : 13.5)	(29.9 : 31.7)	(113.4 : 129.1)	(310.3 : 356.1)	(3.0 : 5.5)	(1.9 : 7.4)	(20.6 : 154.0)	(39.1 : 284.2)	(-212.6: -4.9)
Bloom 2	1006.6[b]	2.9[ab]	4.0	15.9[ab]	31.8[a]	120.3[b]	312.3[b]	8.7[b]	2.3[b]	87.0[b]	123.1[b]	−36.1[a]
(142–156)	(650.3 : 1388.9)	(2.0 : 3.9)	(2.7 : 5.1)	(15.0 : 16.7)	(30.9 : 32.4)	(104.2 : 134.5)	(269.7 : 355.0)	(2.0 : 14.3)	(1.9 : 2.8)	(7.9 : 229.6)	(9.1 : 277.9)	(-80.0: -1.3)
Bloom 3	426.4[b]	3.2[ab]	3.6	19.9[b]	32.3[ab]	113.5[b]	270.0[a]	7.5[b]	4.6[a]	44.3[b]	74.5[b]	−30.1[a]
(169–216)	(136.3 : 783.5)	(2.0 : 4.4)	(1.5 : 9.7)	(16.5 : 22.0)	(30.8 : 33.5)	(84.6 : 146.8)	(202.7 : 349.8)	(2.6 : 16.2)	(2.9 : 8.8)	(-172.1 : 197.1)	(0.1 : 411.2)	(-214.1: -0.1)
Bloom 4	698.6[b]	2.3[b]	2.8	20.5[b]	33.6[b]	96.8[ab]	237.6[a]	5.0[b]	3.1[ab]	2.2[ab]	6.4[a]	−4.2[b]
(236–240)	(570.7 : 817.6)	(1.9 : 3.1)	(2.0 : 4.4)	(19.7 : 20.9)	(33.6 : 33.6)	(94.4 : 99.1)	(234.3 : 241.7)	(3.3 : 6.5)	(2.8 : 3.4)	(-1.2 : 6.2)	(1.6 : 12.0)	(-6.6: -2.5)

Included mean water column irradiance I_m (W h m^{-2} d^{-1}), tidal range (m), wind speed (m s^{-1}), temperature (°C), salinity, dissolved oxygen (% and μmol L^{-1}), chlorophyll '*a*' (μg L^{-1}) and turbidity (FNU). Calculated productivity rates: NCP, GPP and ER in mmol O_2 m^{-2} d^{-1}.
Letters in superscript indicate a significant difference from one/all other groups (Dunn's test; $p < 0.05$).
Bloom events are expressed in Julian Day.

monthly average values of ~7 °C during January and February (Fig. 2a), then steadily increasing until reaching an average of 20.3 °C for July and August and later decreasing to a value of 8.7 °C in December 2019.

Salinity showed low variation across the whole year, with an average of 31.8 ± 1.2 (Fig. 2b). Some differences, although not significant, were found over 24 h periods, but as seen in previous studies (Levasseur et al., 2007), salinity at this point of the estuary is mainly driven by the semi-diurnal tidal cycle and typically ranges between 28.0 and 32.9.

Oxygen concentration showed a year minimum of 165 μmol L^{-1} during July and a maximum of 450.4 μmol L^{-1} in June (Fig. 2c). The greatest daily variability was observed between April–July, with days outside this period presenting up to six times less daily standard deviation (data not shown). The oxygen concentration during the first 3 months remained at ~300 μmol L^{-1}, while from August to December, a gradual monthly average increase occurred, with averages from 225.2 to 287.3 μmol L^{-1}. An average value of oxygen saturation over the whole year of 100.8% indicated an overall balance in the oxygen saturation (Fig. 2d). Oxygen percentage presented mainly oversaturated conditions between April and July and similar to oxygen concentration, consistently showed the greatest daily variations, with the lowest value in July (71.1%), while the highest in June (183.5%). During the rest of the year, oxygen conditions remained slightly undersaturated. Both oxygen parameters displayed peaks during the high productivity period, comprising days of continuous values > 115% saturation and >300 μmol L^{-1} concentration.

Chl '*a*' showed a clear period of increased concentration from late April to late August (Fig. 2e). Outside of this period, average Chl '*a*' concentration remained below 1.5 μg L^{-1}. Four phytoplankton bloom events of different duration and magnitude were observed (Table 2): (i) in late April, a peak dominated by the colonial phytoplankton *Phaeocystis* was observed for 14 days with an overall average of 4.2 μg L^{-1} and, (ii) at the end of May, a bloom comprising of the diatom *Guinardia delicatula* was sustained for 15 days with an average of 8.7 μg L^{-1} and reached a maximum value of 27.1 μg L^{-1} (iii) The most prolonged bloom was observed for about 48 days during June–July and was mainly attributed to the photosynthetic ciliate *Mesodinium rubrum*, presenting the year maximum value of 28.3 μg L^{-1} and an event average of 7.5 μg L^{-1} and finally, (iv) a short bloom was observed at the end of August for 5 days with a mean concentration of 5 μg L^{-1}. The major bloom events in late April, early June and late August developed following a spring tide and peaked during the next neap tide (Fig. 2). The more prolonged bloom dominated by *Mesodinium rubrum* in July started on a neap tide in late June but was then sustained over two further spring/neap periods until late July.

Turbidity measurements ranged between 1.2 and 16.6 FTU, with a marked period from May to July of low turbidity when daily averages remained below 6 FTU (Fig. 2f). Increased daily variation in turbidity was observed from September to December, but this could have been caused by some biofouling of the turbidity sensor since Chl '*a*' for this period remained unaffected. Highest turbidity values corresponded to maximum tidal ranges during peak spring tides (Fig. 2f).

The first two weeks of March, showed high wind speeds in comparison to the rest of the year, with sustained daily values above 6 m s^{-1} and gusts reaching up to 16.8 m s^{-1}. Following this a period lasting until the end of July of lower wind speeds (>5 m s^{-1}) was identified (Fig. 2g).

For I_0, values ranged between 165.9 and 3313.6 W h m^{-2} d^{-1} in January and July, respectively (Fig. 3a). A sudden increase in values was observed at the end of March, reaching slightly above 2000 W h m^{-2} d^{-1} but then decreasing to ~1300 W h m^{-2} d^{-1} for two weeks, before increasing again and remaining mainly above 2000 W h m^{-2} d^{-1} for the period between April and August.

I_m showed a large variation throughout the year, with a monthly range from 55.9 W h m^{-2} d^{-1} in November to 1004.6 W h m^{-2} d^{-1} in May (Fig. 3b). Sustained values above the annual average of 321.4 W h m^{-2} d^{-1} were observed from April to late September, after which a drop in values remained for the rest of the year. An exceptionally high I_m period occurred in late April and throughout the whole of May, with three different events, lasting from 3 to 9 days, of sustained values above 1000 W h m^{-2} d^{-1}.

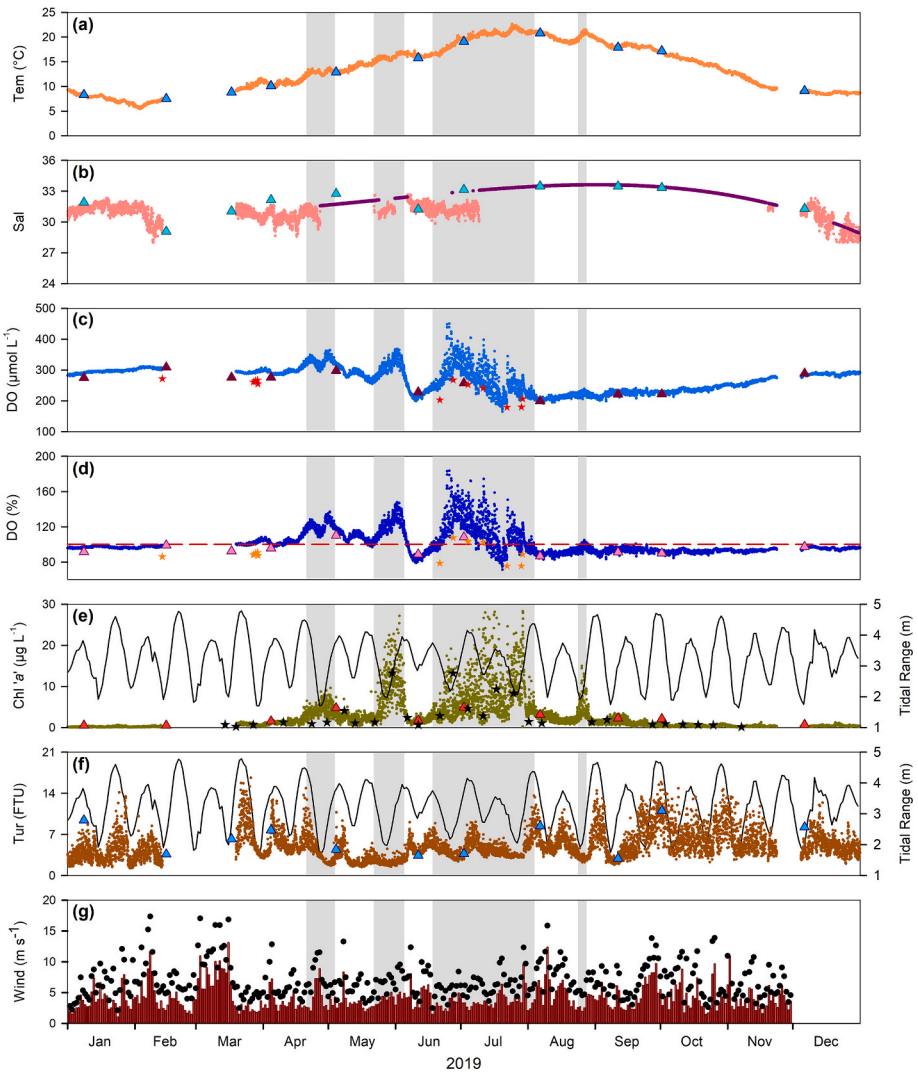

Fig. 2. Hourly time series of environmental conditions at the Xylem Data Buoy in Southampton Water in 2019: (a) temperature, (b) salinity, (c) DO in concentration and (d) DO in percentage saturation, (e) chlorophyll '*a*', (f) turbidity and (g) wind speed, represented as daily mean in vertical bars ▮ and maximum daily values in black circles ●. In a to g, the 4 major blooms identified are shown as a grey background ▮. In d, the red dashed line -- represents 100% of saturation. In c, d and f discrete samples are shown as ★ in different colours. In e and f, the daily tidal range is indicated with a black line. In a to f, Environmental agency sampling points are shown as triangles ▲ in different colours. (For interpretation of the references to colour in this figure legend, the reader is referred to the Web version of this article.)

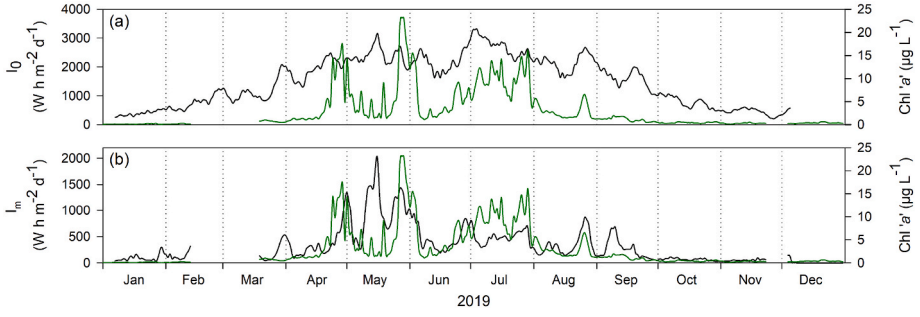

Fig. 3. Temporal variations (7-day running mean) in (a) surface irradiance I_0 and (b) mean water column irradiance I_m with daily mean chlorophyll '*a*' concentration included in (a) and (b) as a green line.– (For interpretation of the references to colour in this figure legend, the reader is referred to the Web version of this article.)

3.2. Fluctuation of productivity rates

Estimated daily values of ER are presented in Fig. 4. Calculated values ranged from 0.1 (June) to 437.5 (August) mmol O_2 m^{-2} d^{-1} with a yearly average of 37.6 mmol O_2 m^{-2} d^{-1}. ER rates did not show a particularly well defined seasonality with occasional periods of ~7 days of peaks in activity throughout the year, notably from May to November. From August to October, monthly values were above 50.0 mmol O_2 m^{-2} d^{-1}. Conversely, March presented a particularly low monthly value of 2.9 mmol O_2 m^{-2} d^{-1} (although only 12 days of estimates were available).

GPP presented an annual daily average of 36.7 mmol O_2 m^{-2} d^{-1} and varied from 0.1 to 411.2 mmol O_2 m^{-2} d^{-1} with both values occurring in the second half of June, only 11 days apart, as seen in Fig. 4. A period of

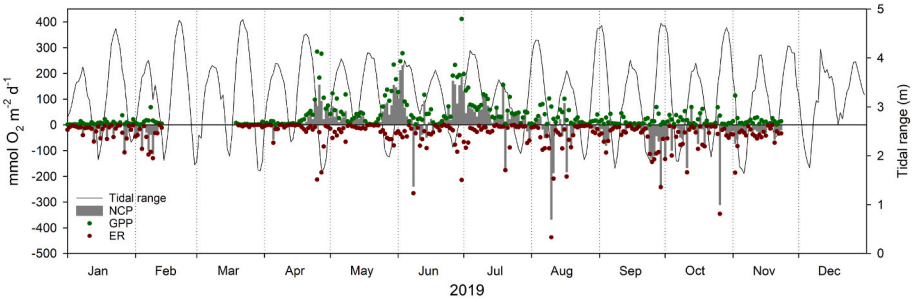

Fig. 4. Calculated daily net community production NCP (vertical bars ▮), ecosystem respiration ER (red circles ●) and gross primary production GPP (green circles ●). Respiration data are displayed as negative values. Change in the daily tidal range is indicated — as a black continuous line. (For interpretation of the references to colour in this figure legend, the reader is referred to the Web version of this article.)

increased productivity was noted from late April to mid-August, with the average productivity rate for this time being 58.6 mmol O_2 m^{-2} d^{-1}, compared to only 11.1 mmol O_2 m^{-2} d^{-1} for the rest of the year. In addition, daily values outside this period were below 100.0 mmol O_2 m^{-2} d^{-1}, while ~20% of daily observations from April to May were above this rate.

Positive daily values of NCP indicate net autotrophy within the water column while negative values suggest net heterotrophy. NCP showed a relatively balanced annual average of −0.8 mmol O_2 m^{-2} d^{-1}. Positive NCP estimations exhibited a seasonal pattern with a highly productive period from April to July (Fig. 4), reflecting net autotrophic conditions with an average of +34.8 mmol O_2 m^{-2} d^{-1} across the 4-month period. The highest positive NCP value of the year (+229.6 mmol O_2 m^{-2} d^{-1}) was observed at the end of a 57-day period of continuous autotrophic conditions, that averaged +44.1 mmol O_2 m^{-2} d^{-1}, and matched the peak in Chl '*a*' concentration at the end of May. This peak was followed closely by a second observed in late-June (+197.1 mmol O_2 m^{-2} d^{-1}), when an additional extended autotrophic period (29 days) averaged +72.2 mmol O_2 m^{-2} d^{-1}. Heterotrophic conditions were nearly absent from March to May, presenting less than ~15% of total observations in this period. However, in August (−366.8 mmol O_2 m^{-2} d^{-1}) and October (−309.8 mmol O_2 m^{-2} d^{-1}) some high negative daily rates of NCP were estimated. From August to November, a heterotrophic state averaging −30.0 mmol O_2 m^{-2} d^{-1} was calculated.

3.3. Relation between environmental conditions and bloom events

Spearman's rank coefficients analysis (Table 1, $p < 0.05$) showed that NCP was strongly positively ($\rho > 0.55$) correlated with I_m, DO in percentage and concentration of Chl '*a*' and negatively correlated ($\rho = 0.43$) with turbidity. GPP showed a strong positive correlation ($\rho > 0.55$) with Chl '*a*' concentration. Moderate positive correlations were also found between GPP and I_m ($\rho = 0.40$), average wind speed ($\rho = 0.47$) and temperature ($\rho = 0.41$). ER was found to strongly negatively correlate with average wind speed ($\rho > 0.55$).

For this study, a major bloom was considered when 1-h average values of Chl '*a*' concentration were sustained above 10 μg L^{-1} and when the biomass gain corresponded to NCP values >+20 mmol O_2 m^{-2} d^{-1}. In order to evaluate differences among parameters during bloom events and the rest of the days studied (identified as low productivity periods LPP), a Kruskal-Wallis analysis ($p < 0.05$) was conducted, paired with Dunn's test ($p < 0.05$) to identify specific groups (Table 2). Both Chl '*a*' and I_m showed a clear separation between bloom groups and LPP, presenting higher average values during bloom events, particularly during Bloom 2. On average, oversaturated oxygen values were observed during Bloom 1, 2 and 3, while during Bloom 4 and LPP, water was slightly undersaturated. For NCP, Bloom 4 and LPP presented average values closer to production balance (=0), while Bloom 1, 2 and 3 showed mean values reflecting a more autotrophic state (>0). Bloom 4 was grouped with LPP for GPP data due to its lower mean value. For ER, Bloom 4 presented a tighter range and lower average than the other groups; hence was separated. Grouping blooms based on temperature placed those occurring during summer (Bloom 3 and 4) and those in winter-spring periods (LPP and Bloom 1) in different groups, with Bloom 2 (late spring) overlapping among the two groups (Table 2).

Further analysis of the influence of environmental conditions on major bloom events is shown in the PCA (Fig. 5). The first two principal components accounted for ~58% of the total variance. Major bloom events related strongly ($R^2 > 0.80$) to I_0, I_m, O_2% and Chl '*a*', and moderately ($R^2 > 0.68$) to GPP and NCP; parameters related to the distribution across PC1 and associated to autotrophic conditions. The river input to the estuary was explained by the spreading of data in PC2, being the main contributors ($R^2 > 0.84$) temperature and salinity, and inversely ($R^2 < -0.81$) river inflow and [O_2]. River flow reflected a weaker influence on bloom event separation; however, Bloom 3 was to some extent related to daily rates during lower riverine inflow. The classification of blooms through the PCA analysis related events negatively to turbidity and tidal range and did not reflect any major influence of river inflow, or wind speed.

4. Discussion

4.1. Drivers of phytoplankton bloom events

Blooms are a fundamental feature of phytoplankton dynamics, defined as events of fast growth and accumulation of biomass, occurring at different magnitudes and duration according to environmental conditions (Shi et al., 2016). Three major phytoplankton bloom events were observed in the mid Southampton Water estuary between late April and the beginning of August 2019, plus a fourth minor bloom detected at the end of August.

Daily peaks in Chl '*a*' recorded during bloom events in the present study compare well with previous observations in the estuary (Iriarte and Purdie, 2004; Torres-Valdés and Purdie, 2006), where values reached nearly 20 μg L^{-1} during spring blooms. The magnitude of coastal phytoplankton blooms is highly variable across the world; ranging from coastal ecosystems with typically low concentrations of Chl '*a*' such as the Thau Lagoon (France) presenting mean values between 2.8 and 3.6 μg L^{-1} during intense bloom events (Trombetta et al., 2019) to the Lagoon and Bay of Bizerte (Tunisia) described by Salhi et al. (2018) displaying more comparable maximum mean values during a summer bloom (15.8 and 8.5 μg L^{-1}). It is also possible to find highly eutrophicated systems like the Sundays Estuary in South Africa where exceptional maximum chlorophyll values during blooms above 100 μg L^{-1} have been reported (Lemley et al., 2018a, 2020).

Nutrient input from runoff can supply ecosystems with nutrients, stimulating phytoplankton production and leading to the accumulation of biomass and bloom formation (Cloern and Jassby, 2010; Trombetta et al., 2019). In the Southampton Water estuary, dissolved inorganic nitrogen, phosphorus and silicate measurements from surface water

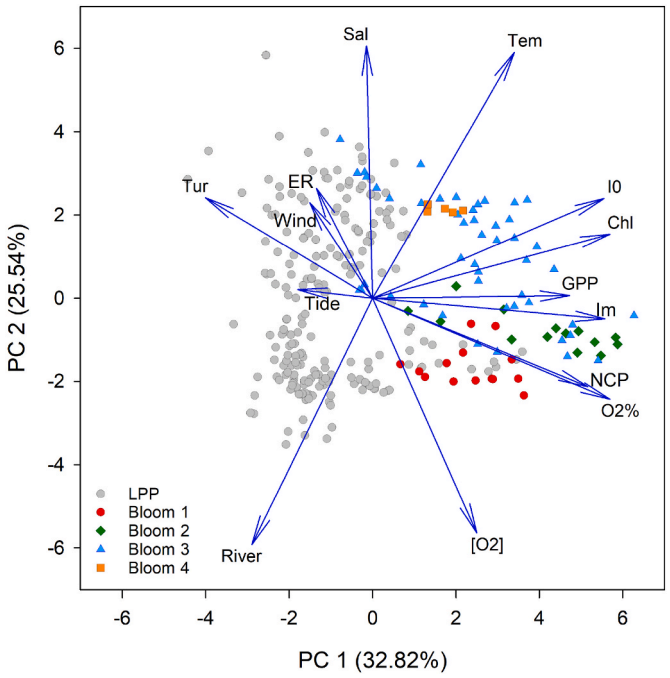

Fig. 5. Principal Component Analysis (PCA) of environmental conditions. The data clustering and the primary (PC1: 32.82% of the variance) and secondary (PC2: 25.54% of the variance) axes represent 58.36% of the total variance. Bloom events have been used as factors to illustrate the clusters: Low productivity period LPP (studied days without blooms) (grey circles ●), Bloom 1 (red circles ●), Bloom 2 (green diamonds ♦), Bloom 3 (blue triangles ▲) and Bloom 4 (orange squares ■). Arrows → represent the variable and the direction of an arrow indicates its relation with the Principal Component (PC) and other variables. Tem = temperature, Sal = salinity, Chl = chlorophyll '*a*', I0 = surface water irradiance, Im = mean water column irradiance, O2% = DO in percentage saturation, [O2] = DO concentration, Wind = wind speed, Tur = turbidity, Tide = tidal range, River = river inflow, GPP = gross primary production, ER = ecosystem respiration and NCP = net community production. (For interpretation of the references to colour in this figure legend, the reader is referred to the Web version of this article.)

samples collected near to the data Buoy remained relatively high throughout the winter and early spring (Kifle and Purdie, 1993) (see supplementary Figure A2). There was then a reduction in concentration of all three nutrients during April with phosphate concentration becoming close to undetectable during the *Phaeocystis* bloom in late April/early May. All three nutrients were then depleted to minimum concentrations at the end of May during the diatom bloom dominated by *Guinardia delicatula* that coincided with neap tides as previously reported by Kifle (1992) and Murty et al. (2017). Then during June when chlorophyll concentrations decreased to less than 5 μg L^{-1}, all three nutrients showed an increase in concentration. During the peak of the *Mesodinium rubrum* bloom in early to mid-July both nitrate and phosphate concentrations were depleted and remained at almost undetectable concentrations.

One of the main factors limiting water column primary production is light availability, in shallow and turbid coastal systems (Brito and Newton, 2013). A comparison between the temporal variation of average daily Chl '*a*' concentration and I_m (Fig. 6a), showed that Chl '*a*' values above 10 μg L^{-1} only occurred when I_m was greater than 280 W h m^{-2} d^{-1}. A similar comparison between NCP values and I_m (Fig. 6b) resulted in positive values, therefore production exceeding respiration, when I_m was above 450 W h m^{-2} d^{-1}. Riley (1967), proposed a theoretical I_m critical value for a sustained increase in phytoplankton biomass, in temperate coastal and estuarine waters, of 200 W h m^{-2} d^{-1}, a threshold value below that found in the present study. However, previous research in Southampton Water (Iriarte and Purdie, 2004) found that Chl '*a*' levels above 10 μg L^{-1} occurred, when I_m averaged for the previous 7 days exceeded 380 W h m^{-2} d^{-1}.

In temperate latitudes, water temperature is a critical parameter influencing phytoplankton bloom development (Lemley et al., 2018b; Trombetta et al., 2019). Furthermore, phytoplankton growth rates increase with temperature, almost doubling with each 10 °C rise (Rose and Caron, 2007). Given the range of temperature observed during 2019 in Southampton Water (5.7–22 °C), phytoplankton growth rates will have increased by more than double during the annual period studied. A comparison of temporal variation in water temperature against daily average Chl '*a*' concentration (Fig. 6c) and NCP (Fig. 6d) found that bloom conditions only occurred when temperature values were above 11.9 °C for both parameters. A similar result was reported by (Iriarte and Purdie, 2004) in their previous 5-year study where all major bloom events in Southampton Water occurred when water temperature was greater than 12 °C. An identical reference value of 12 °C was found by (Carstensen et al., 2015) for coastal sites in the Rhine-Meuse-Scheldt delta and the Wadden Sea, indicating phytoplankton communities of temperate coastal ecosystems, at comparable latitudes, tend to bloom at around the similar threshold temperature. When compared against a coastal ecosystem at a lower latitude (southern France), the spring bloom generally occurred at a slightly increased temperature of 14 °C (Trombetta et al., 2019).

Water level data analysed showed a positive correlation (data not shown) between tidal range and turbidity, indicating that turbidity in the system generally increased during spring tides. Bucci et al. (2012) reported phytoplankton summer blooms in the São Vicente estuary (Brazil) usually occurred towards the end of neap tides, but no significant correlation with tidal cycles was found. This lack of correlation with tidal range, in addition to the strong correlations between phytoplankton peaks and I_m and temperature, indicate that blooms in the Southampton Water estuary are not only regulated by turbulent mixing due to tides but a combination of factors affecting the solar radiation attenuation throughout the water column (Cloern et al., 2014). In most shallow estuaries where the neap-spring cycle is present, fortnightly patterns of reduced mixing during neap tides can be observed (Carstensen et al., 2015), and it is during these periods that phytoplankton net biomass growth is enhanced. The same pattern was reported by Cloern (1996) for the San Francisco Bay; a system with similar depth (~10 m), however, a smaller tidal range (2 m) than Southampton Water. Nevertheless, fluctuations in phytoplankton biomass were also related to the neap-spring cycle for all the spring blooms observed in their study, with phytoplankton biomass increasing during extremely weak neap tides and increased light availability.

4.2. Net community production

High-frequency DO measurements represent a useful opportunity to link productivity rate dynamics and net community production response to short-period changes in environmental conditions, as well as episodic events, such as storms or increased river inputs (Staehr et al., 2012). The annual average rate of NCP for Southampton Water of −0.8 mmol O_2 m^{-2} d^{-1} showed an overall more or less balance between GPP and ER, leaning slightly towards a heterotrophic state. A more heterotrophic annual average value of −5 mmol O_2 m^{-2} d^{-1} was reported for a shallow bank in the mouth of the Thames estuary, calculated using the open diel method (Hull et al., 2016). Reports of more highly heterotrophic ecosystems are widely described in the literature: such as the Ria Formosa Lagoon, South Portugal with DO dynamics used to calculate an annual value of −244 mmol O_2 m^{-2} d^{-1} (Cravo et al., 2020) and the use of the LOICZ biogeochemical model applied to four different coastal lagoons in the Gulf of California reported all of them to be heterotrophic for the time studied (Valenzuela-Siu et al., 2007). Caffrey et al. (2014) calculated the annual NCP, for three different estuaries in the Gulf of Mexico, and found all sites were net heterotrophic for most of the year with the greatest heterotrophy during the summer. On the other hand, an

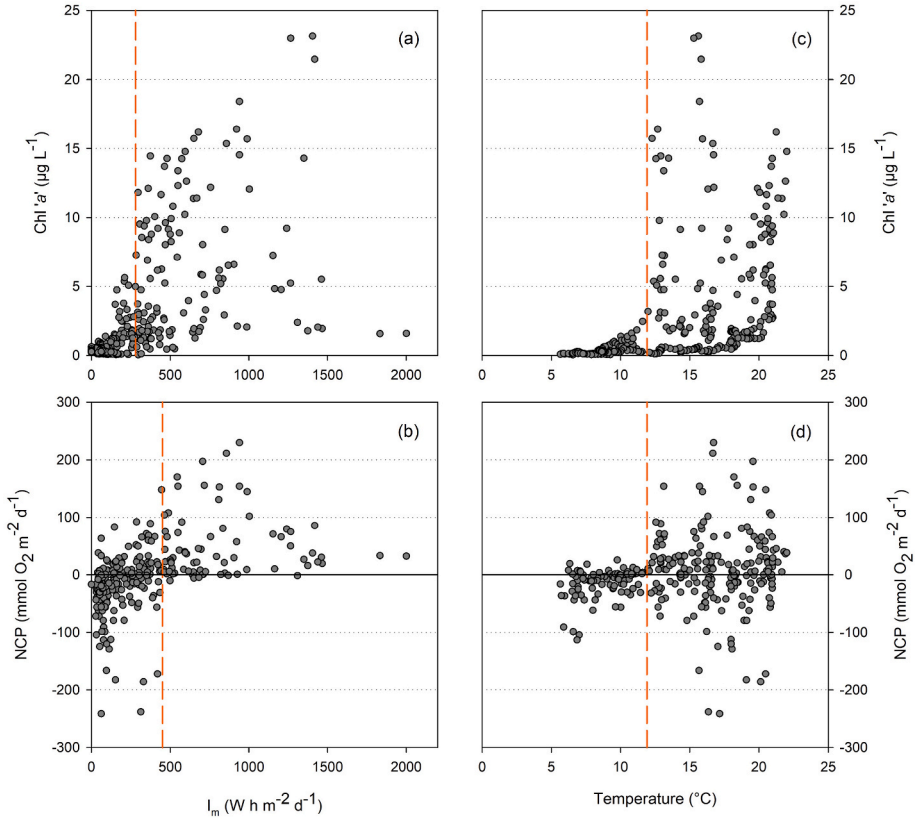

Fig. 6. Daily mean water column irradiance I_m compared with (a) daily chlorophyll '*a*' and (b) net community production NCP; and daily temperature averages compared with (c) daily chlorophyll '*a*' and (d) net community production NCP. References lines -- for water column irradiance I_m of 280 (a) and 450 W h m^{-2} d^{-1} (b), and temperature of 11.91 °C (c and d) were added in.

example of an ecosystem inclining to an autotrophic state is that reported by Haskell et al. (2019) in a productive coastal zone in southern California where NCP values of +0.16 and + 0.18 mmol O_2 m^{-2} d^{-1} were calculated for 2013 and 2014, respectively through glider-measured oxygen concentrations.

Results from the current study showed a noticeable pattern of NCP behaving more similarly to GPP than to ER (see supplementary Figure A4), and both showing a strong correlation to Chl '*a*' concentration (Table 1), suggesting productivity rates could be regulated by factors influencing autotrophic processes. The same tendency of GPP influencing NCP trends more strongly and correlations with Chl '*a*' were observed by Agusti et al. (2018) in their study of the productive Matilda Bay in Australia, where they found that over an annual period, ER rates were less variable than GPP rates. Lack of correlation between ER and Chl '*a*', while presenting a strong relation to GPP, was also observed by Murrell et al. (2018) in their study of a river-dominated estuary located in the Gulf of Mexico.

The range of ER values found in the current study is broader (0.1–437.5 mmol O_2 m^{-2} d^{-1}) than that reported based on O_2 incubations for Southampton Water by Hopkinson and Smith (2005) ranging from 1.0 to 246 mmol O_2 m^{-2} d^{-1}. Moreover, ER showed no clear seasonal pattern, while GPP produced maximum rates during the spring-summer period (Fig. 4). This was reflected in moderate correlations between GPP and temperature and I_m (Table 1), with higher values converging during summer. Since NCP closely reflected GPP trends (see supplementary Figure A4), the highest positive NCP calculated value of 175 mmol O_2 m^{-2} d^{-1}, was observed in the middle of the spring-summer period. This maximum value is lower than others have reported during spring-summer NCP peaks in the Ria de Vigo, Spain (Alonso-Pérez et al., 2015) and in the mouth of the River Thames (Hull et al., 2016), of ~300 mmol O_2 m^{-2} d^{-1} and 485 mmol O_2 m^{-2} d^{-1}, respectively.

Photosynthetic rates generally present a close relation to light availability in the water column, although coastal ecosystem respiration is sometimes unaffected directly by light levels (Kemp and Testa, 2011). An analysis of NCP and light availability (Fig. 6b) showed that when I_m reached values of 450 W h m^{-2} d^{-1} and above, NCP was consistently positive, indicating at these levels of I_m, productivity was consistently exceeding respiration; hence, the system was net autotrophic.

As shown with Chl '*a*' concentration peaks, NCP daily values during the high productivity period (April to August) were related to neap tides (Fig. 4). During these months, NCP showed a biweekly pattern peaking during the monthly low neap tide. The tidal fluctuation creates weaker mixing conditions during neap tides, leading to enhanced phytoplankton biomass growth. The estuary then, appears strongly autotrophic during these tides and moves to a less autotrophic state, and sometimes, even shifting to heterotrophic conditions with the onset of the spring tide. Nidzieko et al. (2014) reported comparable observations for the tidal creek/marsh area in the deeper main channel of Elkhorn Slough, California. Here net heterotrophic conditions were observed during spring tides and mostly in balance conditions during neap tides, mainly due to the spring tide generating greater horizontal mixing transporting well-oxygenated water from the main channel.

Although our results showed that the Southampton Water estuary presented an overall net heterotrophic annual state in 2019, where input of external organic matter is needed, and CO_2 is released to the atmosphere (Tang et al., 2015), seasonal productivity events shifted this state for a few days and sometimes weeks to autotrophic conditions, particularly during the highly productive period in spring-summer. This change meant that for brief periods, the ecosystem was a strong CO_2 sink and a source of organic matter and oxygen (Lee et al., 2017), consistent with the hypothesis that primary production during these brief episodes is a substantial component of annual primary production (Cloern et al.,

2014). Nevertheless, the link between air-sea CO_2 exchange and the metabolic status of an ecosystem is not always direct, since physical settings like water residence time can play a major role in the coupling of these estimations (Borges and Abril, 2011; Cai, 2011). Short residence times of a few of days, as typically observed in Southampton Water (5–10 days) (Sharples, 2000; Shi, 2000), can flush the water mass quickly enough so that biological activity has little or no effect on air-sea CO_2 fluxes (Gazeau et al., 2005b).

4.3. Method implications

The open diel oxygen method coupled with high-frequency water quality monitoring is a powerful tool to help understand the influence of physical and biological processes on DO changes through time, particularly since the principal biological process influencing the ocean's declining DO concentration is phytoplankton respiration (Robinson, 2019). The increasing availability of improved and affordable instrumentation has made it possible to create high-frequency time-series, from which more reliable estimations of net community production can be derived and evaluate different spatial and temporal variability within ecosystems (Aristegi et al., 2009; Staehr et al., 2012).

As with any method, assumptions must be made in order to apply the approach to different ecosystems and data availability. Since it frames the possibility of applying the open diel method to a particular ecosystem, one of the main assumptions is that the water column monitored must be reasonably homogenous and well mixed (Caffrey et al., 2014). Vertical profiles of temperature, salinity and DO% made previous to the 2019 data time series (see supplementary Figure A3) presented temperature differences between the surface and bottom waters that ranged from 0.1 °C in late April to 2.0 °C in July. DO saturation throughout the water column presented higher variability in August (9%) and did not correspond with the profile presenting the greater temperature variation or the highest temperature (July). Both DO saturation and temperature showed less variability through the water column than data in Murrell et al. (2018) study (26% and ~4 °C).

Among other complications previously encountered using this methodology is the necessity to separate air-sea O_2 exchange (Staehr et al., 2012). Direct measurements of air-water exchange can present great difficulty, and some past works have opted for assumed constant values for similar systems (Caffrey, 2004). Since air-water exchange varies due to surface turbulence, water viscosity and the solubility of O_2 (Holtgrieve et al., 2010); to minimize error propagation, in the present study it was calculated for every time-step (1 h) as a function of diffusion through bubbles and gas transfer velocity, which in turn included the Schmidt number encapsulating influences of water temperature and salinity. However, a correlation between values of calculated ER and wind speed (Table 1) suggest highly negative NCP rates related to wind gusts above 9 m s^{-1} (data not shown), thus, an overestimation of heterotrophic conditions. Although wind gusts can induce sediment resuspension, affecting the magnitude and balance between GPP and ER (e.g. Kemp and Testa, 2011), in the current study this appears to be an overprediction of the biological oxygen production (BOP) in the productivity model. Contributions from partially dissolved bubbles and overestimation in the air-water transfer has been reported previously (Haskell et al., 2019; Hull et al., 2016; Liang et al., 2013).

A second generalisation is that ER rates are assumed constant through the diel cycle since CO_2 fixation through chemoautotrophic processes is usually smaller than that fixed by photosynthesis. In most coastal ecosystems (Testa et al., 2012), processes such as nitrification and photooxidation are assumed to be insignificant compared to estimates of 'night respiration' (Demars et al., 2015). Admittedly, if ER was not constant across the diel cycle this would result in an underestimation of both GPP and ER but would not be reflected in the NCP (Murrell et al., 2018).

Discarding anomalous productivity values (i.e.−GPP or + ER) can result in higher rates of GPP and ER than if all data is used, although it seems to have a minimal effect on NCP results (Caffrey et al., 2014). The percentage of anomalous productivity values in the current study was ~20%, similar to the average found in a study of 26 sites within 14 US estuaries, by Caffrey (2003), where the average reported was 23%; however, percentages ranged between 3% and 69%, with only 5 sites having <30%. Moreover, Collins et al. (2013) used a signal processing approach to try to eliminate dissolved oxygen anomalies in their NCP calculations, yet still reported ~11% anomalous values. It seems very likely that some of these anomalous values may simply coincide with periods of low metabolism, falling below the method detection limit.

There are several methods available to estimate aquatic primary production, but few provide the opportunity to calculate directly continuous productivity rates for long periods at a low cost and fieldwork intensity, and at the same time, make available easy validation using independent estimations, like the open diel oxygen method (Briggs et al., 2018). Climate change and variability in environmental conditions will have an effect on both ER and GPP and, consequently, on NCP (Staehr et al., 2012), therefore, it is vital to increase understanding of how these factors influence productivity rates across a broader range of coastal regions, and at a scale that allows prevention and mitigation management in future years.

5. Conclusions

The collection of high-frequency estuarine water quality data allowed the correlation of abiotic environmental conditions with biological rate processes occurring over different time scales. Two independent variables were used to identify major phytoplankton bloom events in the Southampton Water estuary; Chl '*a*' concentration and calculated rates of NCP from high frequency dissolved oxygen concentrations. The initiation of major phytoplankton bloom events during the spring-summer period were correlated with critical values of temperature above 12 °C and mean water column irradiance I_m greater than 280 W h m^{-2} d^{-1}. Additionally, an analysis of the neap-spring tidal cycle identified that blooms typically developed during neap tides and dissipated during the following spring tide. The tidal cycle creates stronger mixing conditions during spring tides leading to increased turbidity compared with lower mixing, and possible stratification, during neap tides enhancing phytoplankton biomass growth. Annual daily average NCP for the estuary detailed a net heterotrophic state (−0.8 mmol O_2 m^{-2} d^{-1}) but seasonal productive events, shifted this state for several days and sometimes weeks to net autotrophic conditions. The results of this study have demonstrated the opportunity of coupling high-frequency data on estuarine water quality and the use of the open oxygen diel method for a broader understanding of the bloom phenomenon in estuarine and coastal waters. Collectively, these studies can provide predictors of future phytoplankton bloom occurrence across a diversity of aquatic ecosystems.

CRediT authorship contribution statement

Africa P. Gomez-Castillo: Writing – review & editing, Writing – original draft, Software, Investigation, Formal analysis, Data curation, Conceptualization. **Anouska Panton:** Writing – review & editing, Resources, Investigation. **Duncan A. Purdie:** Writing – review & editing, Supervision, Resources, Conceptualization.

Declaration of competing interest

The authors declare that they have no known competing financial interests or personal relationships that could have appeared to influence the work reported in this paper.

Data availability

Data will be made available on request.

Acknowledgements

This work was based on the support from CONACyT (the Mexican National Council for Science and Technology) through the grant 'CONACyT-Gobierno del Estado de Sinaloa' reference 472065 and GSNOCS (Graduate School of the National Oceanography Centre Southampton) that provided funding to the lead author, Africa P. Gomez-Castillo. The research was also supported by a European Regional Development Fund grant as part of the Interreg S-3 EuroHAB Project (https://www.s3eurohab.eu). Water quality data was downloaded from the Water Quality Data Archive via the Environment Agency Open WIMS collection. The authors thank the crew of the RV *Callista* for their skilled work in handling the Data Buoy deployments and supporting discrete sampling. We also thank the Associated British Ports (ABP) Marine Environmental Research for providing sea surface elevation data. For the purpose of open access, the author has applied a CC BY public copyright licence to any Author Accepted Manuscript version arising.

Appendix A. Supplementary data

Supplementary data to this article can be found online at https://doi.org/10.1016/j.ecss.2022.108182.

References

Agusti, S., Vigoya, L., Duarte, C.M., 2018. Annual plankton community metabolism in estuarine and coastal waters in Perth (Western Australia). PeerJ 6, e5081. https://doi.org/10.7717/peerj.5081.

Alonso-Pérez, F., Zúñiga, D., Arbones, B., Figueiras, F.G., Castro, C.G., 2015. Benthic fluxes, net ecosystem metabolism and seafood harvest: completing the organic carbon balance in the Ría de Vigo (NW Spain). Estuar. Coast Shelf Sci. 163 (PB), 54–63. https://doi.org/10.1016/j.ecss.2015.05.038.

Aristegi, L., Izagirre, O., Elosegi, A., 2009. Comparison of several methods to calculate reaeration in streams, and their effects on estimation of metabolism. Hydrobiologia 635 (1), 113–124. https://doi.org/10.1007/s10750-009-9904-8.

Bianchi, T.S., 2012. Estuarine chemistry. In: Day, J.W., Crump, B.C., Kemp, W.M., Yáñez-Arancibia, A. (Eds.), Estuarine Ecology, second ed. Wiley-Blackwell, pp. 39–83.

Bittig, H.C., Körtzinger, A., 2015. Tackling oxygen optode drift: near-surface and in-air oxygen optode measurements on a float provide an accurate in situ reference. J. Atmos. Ocean. Technol. 32 (8), 1536–1543. https://doi.org/10.1175/JTECH-D-14-00162.1.

Borges, A.V., Abril, G., 2011. Carbon dioxide and methane dynamics in estuaries. In: Treatise on Estuarine and Coastal Science. Elsevier Inc, pp. 119–161. https://doi.org/10.1016/B978-0-12-374711-2.00504-0.

Briggs, N., Guemundsson, K., Cetinić, I., D'Asaro, E., Rehm, E., Lee, C., Perry, M.J., 2018. A multi-method autonomous assessment of primary productivity and export efficiency in the springtime North Atlantic. Biogeosciences 15 (14), 4515–4532. https://doi.org/10.5194/bg-15-4515-2018.

Brito, A.C., Newton, A., 2013. Measuring light attenuation in shallow coastal systems. J. Ecosyst. Ecography. https://doi.org/10.4172/2157-7625.1000122, 03(01).

Bucci, A.F., Ciotti, Á.M., Gonçalves Pollery, R.C., de Carvalho, R., Cavalcanti De Albuquerque, H., Tomida, L., Simões, S., 2012. Temporal variability of chlorophyll-a in the sao Vicente estuary. Braz. J. Oceanogr. 60 (4), 485–499.

Caffrey, J.M., 2003. Production, respiration and net ecosystem metabolism in U.S. estuaries. Environ. Monit. Assess. 81 (1–3), 207–219. https://doi.org/10.1023/a:1021385226315.

Caffrey, J.M., 2004. Factors controlling net ecosystem metabolism in U . S . Estuaries. Estuaries 27 (1), 90–101. https://doi.org/10.1007/BF02803563.

Caffrey, J.M., Murrell, M.C., Amacker, K.S., Harper, J.W., Phipps, S., Woodrey, M.S., 2014. Seasonal and inter-annual patterns in primary production, respiration, and net ecosystem metabolism in three estuaries in the northeast Gulf of Mexico. Estuar. Coast 37 (S1), 222–241. https://doi.org/10.1007/s12237-013-9701-5.

Cai, W.J., 2011. Estuarine and coastal ocean carbon paradox: CO_2 sinks or sites of terrestrial carbon incineration? Ann. Rev. Mar. Sci 3, 123–145. https://doi.org/10.1146/annurev-marine-120709-142723.

Carstensen, J., Klais, R., Cloern, J.E., 2015. Phytoplankton blooms in estuarine and coastal waters: seasonal patterns and key species. Estuar. Coast Shelf Sci. 162, 98–109. https://doi.org/10.1016/j.ecss.2015.05.005.

Carrit, D.E., Carpenter, J.H., 1966. Comparison and evaluation of currently employed modifications of the Winkler method for determining dissolved oxygen in seawater; a NASCO report. J. Mar. Res. 24, 286–318.

Cloern, J.E., 1996. Phytoplankton bloom dynamics in coastal ecosystems: a review with some general lessons from sustained investigation of San Francisco Bay, California. In: Reviews of Geophysics, vol. 34. Blackwell Publishing Ltd, pp. 127–168. https://doi.org/10.1029/96RG00986. Issue 2.

Cloern, J.E., Foster, S.Q., Kleckner, A.E., 2014. Phytoplankton primary production in the world's estuarine-coastal ecosystems. Biogeosciences 11 (9), 2477–2501. https://doi.org/10.5194/bg-11-2477-2014.

Cloern, J.E., Jassby, A.D., 2010. Patterns and scales of phytoplankton variability in estuarine-coastal ecosystems. Estuar. Coast 33 (2), 230–241. https://doi.org/10.1007/s12237-009-9195-3.

Collins, J.R., Raymond, P.A., Bohlen, W.F., Howard-Strobel, M.M., 2013. Estimates of new and total productivity in central long island sound from in situ measurements of nitrate and dissolved oxygen. Estuar. Coast 36 (1), 74–97. https://doi.org/10.1007/s12237-012-9560-5.

Cravo, A., Rosa, A., Jacob, J., Correia, C., 2020. Dissolved oxygen dynamics in Ria Formosa Lagoon (South Portugal) - a real time monitoring station observatory. Mar. Chem. 223 https://doi.org/10.1016/j.marchem.2020.103806.

Crawford, D.W., Purdie, D.A., Lockwood, A.P.M., Weissman, P., 1997. Recurrent red-tides in the Southampton water estuary caused by the phototrophic ciliate Mesodinium rubrum. In: Estuarine, Coastal and Shelf Science, vol. 45.

Demars, B.O.L., Thompson, J., Manson, J.R., 2015. Stream metabolism and the open diel oxygen method: principles, practice, and perspectives. Limnol Oceanogr. Methods 13 (7), 356–374. https://doi.org/10.1002/lom3.10030.

Duarte, C.M., Regaudie-De-Gioux, A., 2009. Thresholds of gross primary production for the metabolic balance of marine planktonic communities. Limnol. Oceanogr. 54 (3), 1015–1022.

Emerson, S., Stump, C., Nicholson, D., 2008. Net biological oxygen production in the ocean: remote in situ measurements of O2 and N2 in surface waters. Global Biogeochem. Cycles 22 (3), 1–13. https://doi.org/10.1029/2007GB003095.

Feistel, R., 2008. A Gibbs function for seawater thermodynamics for -6 to 80 °C and salinity up to 120 g kg-1. Deep-Sea Res. Part I Oceanogr. Res. Pap. 55 (12), 1639–1671. https://doi.org/10.1016/j.dsr.2008.07.004.

Feng, M.L., Sun, T., Zhang, L.X., Shen, X.M., 2012. Net ecosystem metabolism simulation by dynamic dissolved oxygen model in yellow river estuary, China. Proc. Environ. Sci. 13 (2011), 807–817. https://doi.org/10.1016/j.proenv.2012.01.074.

Garcia-Corral, L.S., Duarte, C.M., Agusti, S., 2021. Plankton community metabolism in western Australia: estuarine, coastal and oceanic surface waters. Front. Mar. Sci. 7 https://doi.org/10.3389/fmars.2020.582136.

Gazeau, F., Borges, A.V., Barrón, C., Duarte, C.M., Iversen, N., Middelburg, J.J., Delille, B., Pizay, M.-D., Frankignoulle, M., Gattuso, J.P., 2005. Net ecosystem metabolism in a micro-tidal estuary (Randers Fjord, Denmark): evaluation of methods. Mar. Ecol. Prog. Ser. 301, 23–41. https://doi.org/10.3354/meps301023.

Haskell, W.Z., Hammond, D.E., Prokopenko, M.G., Teel, E.N., Seegers, B.N., Ragan, M.A., Rollins, N., Jones, B.H., 2019. Net community production in a productive coastal ocean from an autonomous buoyancy-driven glider. J. Geophys. Res.: Oceans 124 (6), 4188–4207. https://doi.org/10.1029/2019JC015048.

Holtgrieve, G.W., Schindlern, D.E., Branch, T.A., Teresa A'Mar, Z., 2010. Simultaneous quantification of aquatic ecosystem metabolism and reaeration using a Bayesian statistical model of oxygen dynamics. Limnol. Oceanogr. 55 (3), 1047–1063. https://doi.org/10.4319/lo.2010.55.3.1047.

Hopkinson, C.S., Smith, E.M., 2005. Estuarine respiration: an overview of benthic, pelagic, and whole system respiration. In: del Giorgio, P.A., leB Williams, P.J. (Eds.), Respiration in Aquatic Ecosystems. Oxford University Press, pp. 1–328. https://doi.org/10.1093/acprof:oso/9780198527084.001.0001.

Hull, T., Greenwood, N., Kaiser, J., Johnson, M., 2016. Uncertainty and sensitivity in optode-based shelf-sea net community production estimates. Biogeosciences 13 (4), 943–959. https://doi.org/10.5194/bg-13-943-2016.

Iriarte, A., Purdie, D.A., 2004. Factors controlling the timing of major spring bloom events in an UK south coast estuary. Estuar. Coast Shelf Sci. 61 (4), 679–690. https://doi.org/10.1016/j.ecss.2004.08.002.

Jollife, I.T., Cadima, J., 2016. Principal component analysis: a review and recent developments. In: Philosophical Transactions of the Royal Society A: Mathematical, Physical and Engineering Sciences, vol. 374. Royal Society of London. https://doi.org/10.1098/rsta.2015.0202. Issue 2065.

Kanuri, V.V., Gijjapu, D.R., Munnooru, K., Sura, A., Patra, S., Vinjamuri, R.R., Karri, R., 2017. Scales and drivers of seasonal pCO2 dynamics and net ecosystem exchange along the coastal waters of southeastern Arabian Sea. Mar. Pollut. Bull. 121 (1–2), 372–380. https://doi.org/10.1016/j.marpolbul.2017.06.016.

Kemp, W.M., Testa, J.M., 2011. Metabolic balance between ecosystem production and consumption. In: Wolansky, E., McLusky, D.S. (Eds.), Treatise on Estuarine and Coastal Science, vol. 7. Academic Press, Waltham, pp. 83–118.

Kifle, D., Purdie, D.A., 1993. The seasonal abundance of the phototrophic ciliate Mesodinium rubrum in Southampton Water, England. J. Plankton Res. 15 (7), 823–833. Retrieved from. https://academic.oup.com/plankt/article/15/7/823/1472966.

Langdon, C., Garcia-Martin, E.E., 2021. Light and dark dissolved oxygen rate measurements using the Winkler method. In: Vandermeulen, R.A., Chaves, J.E. (Eds.), Aquatic Primary Productivity Field Protocols for Satellite Validation and Model Synthesis, vol. 7. NASA, p. 195.

Lee, J., Kim, S., An, S., 2017. Dynamics of the physical and biogeochemical processes during hypoxia in jinhae Bay, South Korea. J. Coast Res. 33 (4), 854–863. https://doi.org/10.2112/JCOASTRES-D-16-00122.1.

Lemley, D.A., Adams, J.B., Rishworth, G.M., 2018b. Unwinding a tangled web: a fine-scale approach towards understanding the drivers of harmful algal bloom species in a eutrophic South African estuary. Estuar. Coast 41 (5), 1356–1369. https://doi.org/10.1007/s12237-018-0380-0.

Lemley, D.A., Adams, J.B., Rishworth, G.M., Purdie, D.A., 2020. Harmful algal blooms of Heterosigma akashiwo and environmental features regulate Mesodinium cf. rubrum abundance in eutrophic conditions. Harmful Algae 100. https://doi.org/10.1016/j.hal.2020.101943.

Lemley, D.A., Adams, J.B., Strydom, N.A., 2018a. Triggers of phytoplankton bloom dynamics in permanently eutrophic waters of a South African estuary. Afr. J. Aquat. Sci. 43 (3), 229–240. https://doi.org/10.2989/16085914.2018.1478794.

Leterme, S.C., Jendyk, J.G., Ellis, A.v., Brown, M.H., Kildea, T., 2014. Annual phytoplankton dynamics in the Gulf saint vincent, south Australia, in 2011. Oceanologia 56 (4), 757–778. https://doi.org/10.5697/oc.56-4.757.

Levasseur, A., Shi, L., Wells, N.C., Purdie, D.A., Kelly-Gerreyn, B.A., 2007. A three-dimensional hydrodynamic model of estuarine circulation with an application to Southampton Water, UK. Estuar. Coast Shelf Sci. 73 (3–4), 753–767. https://doi.org/10.1016/j.ecss.2007.03.018.

Liang, J.H., Deutsch, C., McWilliams, J.C., Baschek, B., Sullivan, P.P., Chiba, D., 2013. Parameterizing bubble-mediated air-sea gas exchange and its effect on ocean ventilation. Global Biogeochem. Cycles 27 (3), 894–905. https://doi.org/10.1002/gbc.20080.

Mahoney, P.C., Bishop, M.J., 2017. Assessing risk of estuarine ecosystem collapse. Ocean Coast Manag. 140, 46–58. https://doi.org/10.1016/j.ocecoaman.2017.02.021.

Murrell, M.C., Caffrey, J.M., Marcovich, D.T., Beck, M.W., Jarvis, B.M., Hagy, J.D., 2018. Seasonal oxygen dynamics in a warm temperate estuary: effects of hydrologic variability on measurements of primary production, respiration, and net metabolism. Estuar. Coast 41 (3), 690–707. https://doi.org/10.1007/s12237-017-0328-9.

Murty, K.N., Sarma, N.S., Pandi, S.R., Chiranjeevulu, G., Kiran, R., Muralikrishna, R., 2017. Hydrodynamic control of microphytoplankton bloom in a coastal sea. J. Earth Syst. Sci. 126 (6) https://doi.org/10.1007/s12040-017-0867-2.

Needoba, J.A., Peterson, T.D., Johnson, K.S., 2012. Method for the quantification of aquatic primary production and net ecosystem metabolism using in situ dissolved oxygen sensors. In: Tiquia-Arashiro, S.M. (Ed.), Molecular Biological Technologies for Ocean Sensing. Springer Protocols Handbooks. https://doi.org/10.1007/978-1-61779-915-0.

Nidzieko, N.J., Needoba, J.A., Monismith, S.G., Johnson, K.S., 2014. Fortnightly tidal modulations affect net community production in a mesotidal estuary. Estuar. Coast 37 (S1), 91–110. https://doi.org/10.1007/s12237-013-9765-2.

Oczkowski, A., Hunt, C.W., Miller, K., Oviatt, C., Nixon, S., Smith, L., 2016. Comparing measures of estuarine ecosystem production in a temperate new England estuary. Estuar. Coast 39 (6), 1827–1844. https://doi.org/10.1007/s12237-016-0113-1.

Odum, H.T., 1956. Primary production in flowing waters. Limnol. Oceanogr. 1, 102–117.

Panton, A., Couceiro, F., Fones, G.R., Purdie, D.A., 2020. The impact of rainfall events, catchment characteristics and estuarine processes on the export of dissolved organic matter from two lowland rivers and their shared estuary. Sci. Total Environ. 735 https://doi.org/10.1016/j.scitotenv.2020.139481.

Parsons, T., Maita, Y., Lalli, C., 1984. 4.3 - fluorometric determination of chlorophylls. In: Parsons, T., Maita, Y., Lalli, C. (Eds.), A Manual of Chemical & Biological Methods for Seawater Analysis. Pergamon, pp. 107–109. https://doi.org/10.1016/C2009-0-07774-5.

Queste, B.Y., Fernand, L., Jickells, T.D., Heywood, K.J., Hind, A.J., 2016. Drivers of summer oxygen depletion in the central North Sea. Biogeosciences 13 (4), 1209–1222. https://doi.org/10.5194/bg-13-1209-2016.

Riley, G.A., 1967. The plankton in estuaries. In: Lauff, G.H. (Ed.), *Estuaries* (Pp. 316–326). American Association for the Advancement of Science Publication.

Robinson, C., 2019. Microbial respiration, the engine of ocean deoxygenation. Front. Mar. Sci. 5 (January), 1–13. https://doi.org/10.3389/fmars.2018.00533.

Rose, J.M., Caron, D.A., 2007. Does low temperature constrain the growth rates of heterotrophic protists? Evidence and implications for algal blooms in cold waters. In: Limnol. Oceanogr, vol. 52. Issue 2. http://www.aslo.org/lo/toc/vol_52/.

Ruiz-Ruiz, T.M., Arreola-Lizárraga, J.A., Morquecho, L., Mendez-Rodríguez, L.C., Martínez-López, A., Mendoza-Salgado, R.A., 2017. Detecting eutrophication symptoms in a subtropical semi-arid coastal lagoon by means of three different methods. Wetlands 1–14. https://doi.org/10.1007/s13157-017-0944-y.

Salhi, N., Zmerli Triki, H., Molinero, J.C., Laabir, M., Sehli, E., Bellaaj-Zouari, A., Daly Yahia, N., Kefi-Daly Yahia, O., 2018. Seasonal variability of picophytoplankton under contrasting environments in northern Tunisian coasts, southwestern Mediterranean Sea. Mar. Pollut. Bull. 129 (2), 866–874. https://doi.org/10.1016/j.marpolbul.2017.10.029.

Sharples, J., 2000. Water circulation in Southampton water and the solent. In: Collins, M. B., Ansell, K. (Eds.), Solent Science - a Review. Proceedings of Solent Science Conference. Elsevier Science, Southampton, UK, pp. 45–53. Retrieved from. http://eprints.soton.ac.uk/id/eprint/63182.

Shi, J., Liu, Y., Mao, X., Guo, X., Wei, H., Gao, H., 2016. Interannual variation of spring phytoplankton bloom and response to turbulent energy generated by atmospheric forcing in the central Southern Yellow Sea of China: satellite observations and numerical model study. Continent. Shelf Res. 143 (December 2015), 1–14. https://doi.org/10.1016/j.csr.2016.06.008.

Shi, L., 2000. Development and Application of a Three-Dimensional Water Quality Model in a Partially-Mixed Estuary. University of Southampton, Southampton Water, UK.

Srichandan, S., Kim, J.Y., Kumar, A., Mishra, D.R., Bhadury, P., Muduli, P.R., Pattnaik, A. K., Rastogi, G., 2015. Interannual and cyclone-driven variability in phytoplankton communities of a tropical coastal lagoon. Mar. Pollut. Bull. 101 (1), 39–52. https://doi.org/10.1016/j.marpolbul.2015.11.030.

Staehr, P.A., Testa, J.M., Kemp, W.M., Cole, J.J., Sand-Jensen, K., Smith, S.v., 2012. The metabolism of aquatic ecosystems: history, applications, and future challenges. Aquat. Sci. 74 (Issue 1), 15–29. https://doi.org/10.1007/s00027-011-0199-2.

Tang, S., Sun, T., Shen, X.M., Qi, M., Feng, M.L., 2015. Modeling net ecosystem metabolism influenced by artificial hydrological regulation: AN application to the Yellow River Estuary, China. Ecol. Eng. 76, 84–94. https://doi.org/10.1016/j.ecoleng.2014.04.025.

Testa, J.M., Kemp, W.M., Hopkinson, C.S., Smith, S.v., 2012. Ecosystem metabolism. In: Day, W.J., Crump, B.C., Kemp, W.M., Yáñez-Arancibia, A. (Eds.), Estuarine Ecology, second ed. Wiley-Blackwell, pp. 381–416. https://doi.org/10.1002/9781118412787.

Torres-Valdés, S., Purdie, D.A., 2006. Nitrogen removal by phytoplankton uptake through a temperate non-turbid estuary. Estuar. Coast Shelf Sci. 70 (3), 473–486. https://doi.org/10.1016/j.ecss.2006.06.028.

Trombetta, T., Vidussi, F., Mas, S., Parin, D., Simier, M., Mostajir, B., 2019. Water temperature drives phytoplankton blooms in coastal waters. PLoS One 14 (4). https://doi.org/10.1371/journal.pone.0214933.

Uchida, H., Kawano, T., Kaneko, I., Fukasawa, M., 2008. In situ calibration of optode-based oxygen sensors. J. Atmos. Ocean. Technol. 25 (12), 2271–2281. https://doi.org/10.1175/2008JTECHO549.1.

Valenzuela-Siu, M., Arreola-Lizárraga, J.A., Sánchez-Carrillo, S., Padilla-Arredondo, G., 2007. Flujos de nutrientes y metabolismo neto de la laguna costera Lobos, México. Hidrobiologica, 17 (3), 193–202.

Wanninkhof, R., 2014. Relationship between wind speed and gas exchange over the ocean revisited. Limnol Oceanogr. Methods 12 (JUN), 351–362. https://doi.org/10.4319/lom.2014.12.351.

Winkler, L.W., 1888. Die Bestimmung des im Wasser gelosten Sauerstoffes. Ber. Dtsch. Chem. Ges. 21 (2), 2843–2854. https://doi.org/10.1002/cber.188802102122.

Utermöhl, H., 1958. Methods of collecting plankton for various purposes are discussed. SIL Communications, 1953-1996 9 (1), 1–38. https://doi.org/10.1080/05384680.1958.11904091.

Kifle, D. (1992). Seasonal and spatial variations in species composition, abundance, biomass and primary production of phytoplankton in Southampton Water. PhD Thesis, University of Southampton, Southampton, UK.